Title
Tauonic States in the Coulomb Field

Author
Momberger, K.

Publication Date
1996-01-08

LBL-38116
UC-401
Preprint

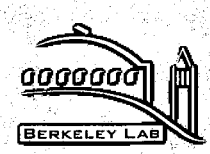

ERNEST ORLANDO LAWRENCE
BERKELEY NATIONAL LABORATORY

Tauonic States in the Coulomb Field

K. Momberger and A. Belkacem
Chemical Sciences Division

January 1996
Submitted for publication

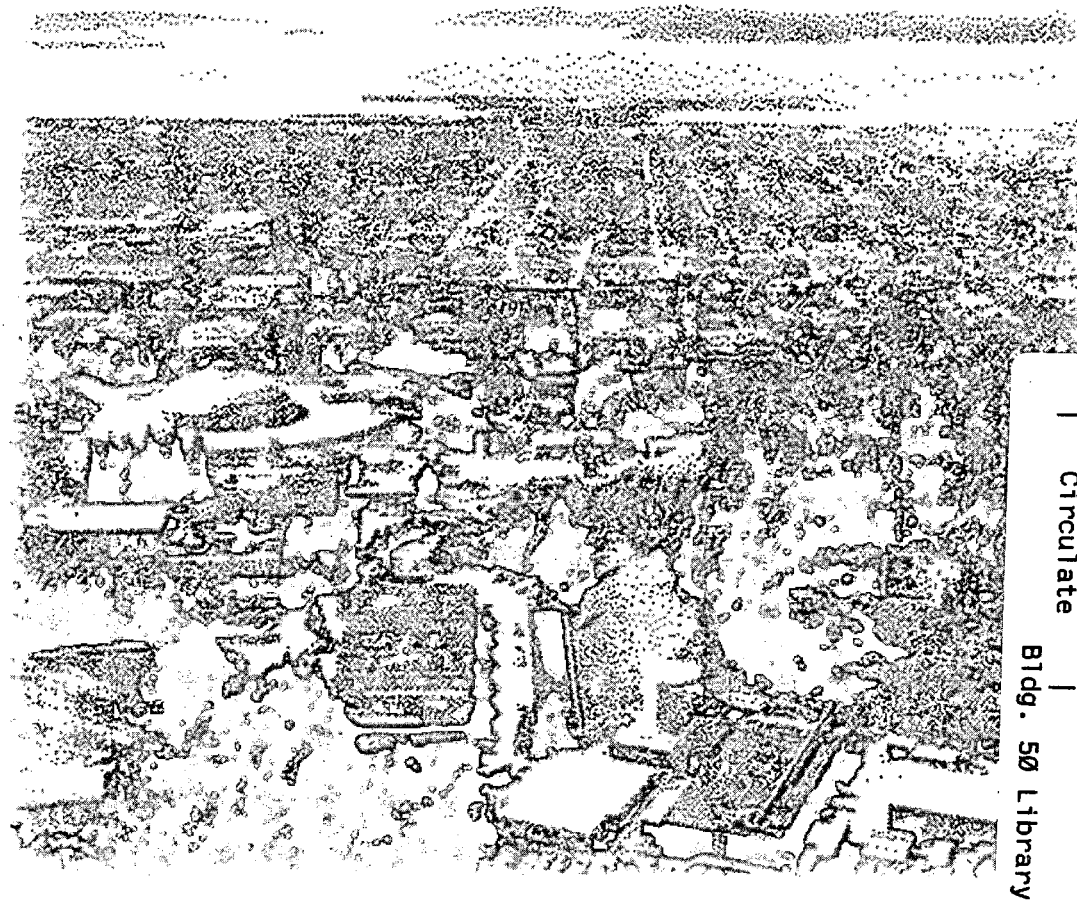

DISCLAIMER

LBL-38116
UC-401

Tauonic States in the Coulomb Field

K. Momberger and A. Belkacem

Chemical Sciences Division
Ernest Orlando Lawrence Berkeley National Laboratory
University of California
Berkeley, California 94720

January 1996

This work was supported by the Director, Office of Energy Research, Office of Basic Energy Sciences, Chemical Sciences Division, of the U.S. Department of Energy under Contract No. DE-AC03-76SF00098.

Tauonic states in the Coulomb field

K. Momberger* and A. Belkacem**
Lawrence Berkeley National Laboratory, MS: 71-259,
1 Cyclotron Road, Berkeley, California 94720
Internet: (*) klausm@lbl.gov, (**) abelkacem@lbl.gov
(January 8, 1996)

We computed relativistic bound and continuum wave functions for a τ lepton in the Coulomb field of an extended nucleus. The solution of the bound state problem provides a gross description of tauonic atoms. The primary purpose of this work is to provide wave functions which will be needed for a computation of electromagnetic $\tau^+ - \tau^-$ pair production cross sections. Due to the heavy mass of the τ relativistic effects are found to be small for the determination of the lower bound state energy eigenvalues. We obtained practically identical energy eigenvalues using a Fermi distribution or a homogeneously charged sphere as a model for the nuclear charge. However, we found slightly different momentum distributions in the wave functions obtained with either charge distribution. The bound state spectra show the uncommon behaviour, that the binding energy within a given shell increases with increasing angular momentum.

I. INTRODUCTION

It has been predicted that at relativistic heavy ion colliders the electromagnetic production of pairs of heavy leptons, such as the μ and τ, can take place [1–3]. It has further been speculated that in non-grazing collisions with small impact parameters the produced negative lepton has a finite probability to end up bound to one of the bare ions. This latter process is potentially a new and unique way to produce exotic atoms of short lived species such as "tauonic" atoms. Traditionally, exotic atoms are produced through slowing down of negative particles ($\mu-$, $\pi-$ or $K-$) in matter where they are first captured into high orbits of the atomic target and then cascade down into lower states by emitting Auger electrons or X-rays. However, the time of production, transport, slowing down and capture of the negative particles into atomic states is of the order of one to a few nanoseconds. As a consequence, this method is not suited for the production of hitherto unobserved exotic atoms with the very short lived τ-lepton whose life time amounts to typically 0.3 *ps*.

The observation of electron-positron pair production with the electron emerging from the collision bound to a heavy ion projectile was already reported in the literature [4,5]. This process termed "capture from pair production" or "bound-free pair production" has been the subject of numerous theoretical papers [6].

In case of heavier leptons, a calculation of muonic bound-free pair production cross sections has been performed in first order perturbation theory using relativistic wave functions for the potential of an extended nucleus, which has shown a strong suppression of this process due to the finite nuclear size [7]. Other perturbation theory calculations for the τ and μ lepton have been carried out using point-like wave functions [2]. μ pair production with capture to a bound state of a colliding ion has also been a subject of intense non-perturbative studies by Wells et al. [8] who solved this problem fully numerically, in principle taking all orders of the interaction into account.

For the heaviest leptons, the earliest estimate for the number of produced τ pairs at RHIC has been given by Gould [1], who assumes a RHIC design of counterrotating beams of fully stripped uranium at 100 GeV/n. His estimate yields a number of 1 τ pair per second, assuming a luminosity of $10^{27} cm^{-2} s^{-1}$, which is undoubtly an upper limit, since finite size effects of the nuclei have been ignored. Taking into account the finite nuclear size will clearly be most important for the τ, as we will elaborate in this paper. In the picture of equivalent photon methods the finite nuclear size (which limits the minimum impact parameter) translates into a severe suppression in the equivalent photon spectrum of photon energies of the order or larger than twice the τ rest mass. These high energies are of course necessary to produce heavy lepton pairs.

An alternate and probably more efficient production of tauonic atoms would be to use real photons impinging on a fixed target. The photons can convert into a pair of τ leptons with the negative partner being created directly in a bound state of the high-Z atomic target. Very intense high energy photon beams (up to 10^{9-10} photons/second) could be obtained through Bremsstrahlung of very intense electron and/or positron beams available at accelerators such as SLAC. Thick high-Z targets could be used to get acceptable rates of production.

A necessary step for the calculation of the cross section for the process of τ pair production with the negative τ created in bound atomic states of the high-Z target is to study the τ states themselves.

A first discussion of τ wave functions motivated by the thought of τ pair production at RHIC has been presented by Weiss [9], who computed bound state solutions of the Schrödinger equation for the potential of a homogeneously charged sphere.

In this paper, we present a relativistic calculation of tauonic bound and continuum wave functions by solv-

ing the radial Dirac equation. Due to its mass of 1784.2 MeV, the orbit of a τ lepton on an inner-shell state will be embedded almost totally inside the nuclear charge. Therefore, we have to consider the Coulomb potential of an extended nucleus. The solution of the bound state eigenvalue problem provides us with a gross description of tauonic atoms. We neglect all further corrections that are standard in the theory of muonic atoms, such as corrections for the reduced mass and QED effects.

As a model for the nuclear charge distribution, we are using a 2-parameter Fermi-distribution and will compare this to a simple homogeneously charged sphere. We are going to solve the problem relativistically, i. e. we are dealing with the Dirac equation.

In the following section, we will briefly describe the methods to solve the bound state eigenvalue problem and to calculate the continuum states. These methods are standard and can be found in the theory of muonic atoms [10] and heavy-ion collisions [11]. In section 3, we will present result for the bound and continuum states.

II. NUMERICAL PROCEDURE

In the standard representation of the Dirac spinor in a spherical symmetric field [12], the radial functions $g(r), f(r)$ obey the radial Dirac equation ($\hbar = m = c = 1$)

$$\begin{aligned} \frac{d\,G}{d\,r} &= -\frac{\kappa}{r}G + (E+1-V)\,F \\ \frac{d\,F}{d\,r} &= -(E-1-V)\,G + \frac{\kappa}{r}F \end{aligned} \tag{2.1}$$

where F is $rf(r)$ and G is $rg(r)$. $V(r)$ is the radial dependence of the central potential. We will use two kinds of potentials for the calculations presented in this paper. The first is the potential of the homogeneously charged sphere, which is given analytically as follows:

$$V(r) = \begin{cases} -\frac{Ze^2}{2R_0}(3 - r^2/R_0^2) & \text{for } r \le R_0, \\ -\frac{Ze^2}{r} & \text{for } r > R_0 \end{cases} \tag{2.2}$$

The second is the potential generated by a Fermi charge distribution and has to be computed numerically. We are using a 2-parameter Fermi distribution which is given by

$$\rho(r) = \frac{N}{1+\exp(4\ln 3\ (r-c)/t)} = \frac{N}{1+\exp(n(r/c-1))} \tag{2.3}$$

where c is the half-density radius and t is the skin thickness parameter, which is defined as the distance over which the charge density drops from 90% to 10% of its maximum value. c and t are related to n by $t = (4c/n)\ln 3$. The Coulomb potential connected to this charge distribution has to be computed numerically according to the following expression:

$$V(r) = -4\pi e^2 \left[\frac{1}{r}\int_0^r \rho(r')r'^2 dr' + \int_r^\infty \rho(r')r'dr'\right] \tag{2.4}$$

Making use of the normalization condition

$$4\pi \int_0^\infty r^2\rho(r)dr = Z \tag{2.5}$$

the normalization factor N can be expressed through c and t [10]:

$$N = \frac{3Z}{4\pi}\frac{1}{c^3 + (\frac{\pi t}{4\ln 3})^2 c} \tag{2.6}$$

The procedure to solve the bound states eigenvalue problem has been developed in the context of self-consistent field methods [13] and has also been applied in the field of heavy-ion collisions [11] and muonic atoms [10]. The range of integration from $r_{min} \approx 0$ to some large value r_{max} is split into an inner and an outer region at the matching radius r_{match}, which is somewhat arbitrarily chosen to be the classical turning point given by

$$r_{match} = Ze^2/(1 - E_{start}) \tag{2.7}$$

where E_{start} is a first guess for the energy eigenvalue. Under the assumption that the charge distribution around r_{min} is practically constant, the starting values at r_{min} can be taken from a series expansion given by Rose [12]. At r_{max} the starting values are taken from the asymptotic behaviour of the solutions for g and f in the pure Coulomb field:

$$F = -\sqrt{(1-E)/(1+E)}\ ; \quad G = 1 \tag{2.8}$$

The inward integration is performed from r_{min} to r_{match} and the outward integration from r_{max} to r_{match}. The mismatch at r_{match} is determined to estimate a correction for E_{start}. Following [13], this correction is assumed to be

$$\Delta E = \lim_{\epsilon\to\infty} \frac{G(r_{match})[F(r_{match}+\epsilon) - F(r_{match}-\epsilon)]}{\int_{r_{min}}^{r_{match}}[F^2+G^2]dr + \int_{r_{match}}^{r_{max}}[F^2+G^2]dr} \tag{2.9}$$

This correction is added to the first guess of the eigenvalue and the procedure is continued until the change in the eigenvalue is negligible. Additionally, the solution has to be checked for the presence of the correct number of nodes. In case of electronic states, the first guess E_{start} usually can be taken from Sommerfeld's fine structure formula. In case of μ and τ leptons, this formula is too far off, so that a proper starting value has to be searched for. For the homogeneous charge distribution, this search can be automatized by systematically

increasing the nuclear radius from 0 to its actual value. Finally, the solutions have to be normalized numerically, which is being done by Gauss-Legendre quadrature.

Since in case of continuum states we do not have to deal with an eigenvalue problem, the numerical procedure is much more straightforward. The numerical integration of the radial equations 2.1 is performed from r_{start} to any arbitrary value of r, using the unnormalized starting values from Rose's [12] series expansion. In order to assure proper normalization of the wave function according to

$$\int_0^\infty r^2 dr \; [f_E(r) f_{E'}(r) + g_E(r) g_{E'}(r)] = \delta(E - E') \tag{2.10}$$

two different methods can be found in the literature:
i) the radial wave functions are integrated up to the asymptotic region and the normalization can be obtained by comparison to the known expressions of the normalized, asymptotic functions. This method is very simple, however, the accuracy of the normalization is limited to about 1% [14,15].
ii) the normalization is obtained at a single point which is sufficiently far outside the charge distribution that deviation from a pure Coulomb potential can be neglected. For a pure Coulomb, the expressions for the normalized wave functions are known analytically and can be evaluated to determine the normalization factor. With this more sophisticated method, an accuracy better than 10^{-10} can be achieved [14,16]. For tauonic wave functions however, the latter method becomes rather delicate, so that we have been using the first method for the results presented here.

III. RESULTS FOR TAUONIC LEAD

Although the original RHIC design assumes uranium ions, we present results for a nucleus of lead ^{208}Pb, for which the assumption of a spherical symmetric charge distribution is more realistic. For the Fermi distribution of a lead nucleus we used the parameters $c = 6.74\ fm$ and $t = 2.0\ fm$, which have determined from muonic atom X-ray data [10]. For the homogeneously charged sphere, we defined the radius according to $R_0 = r_0\, A^{1/3}$. The parameter r_0 has been set to 1.195788 fm, which results in a radius $R_0 = 7.085\ fm$. . With this choice of r_0, the homogeneously charged sphere and the Fermi distribution both yield the same root mean square radius for the charge distribution $< r^2 >^{1/2} = 4\pi \int_0^\infty \rho(r) r^4 dr$, namely 5.48 fm. Therefore, this radius of a homogeneously charged sphere is called the "equivalence radius" of the Fermi distribution. Unless otherwise stated, we are using natural units ($\hbar = m = c = 1$), which means energies are measured in units of the rest mass mc^2 of the τ of 1784.2 MeV and the unit length is the τ's reduced Compton wavelength of $\lambda = 0.1106\ fm$.

A. Inner shell states

In table I the eigenenergies of tauonic lead are displayed for the K-, L-, M-shell and the $4s$, $5s$ and $6s$ states. The results for the Fermi distribution are compared to the homogeneously charged sphere and to Sommerfeld's fine structure formula (point nucleus). The eigenenergies obtained with the homogeneously charged sphere and the Fermi distribution are very close. In comparison to the point nucleus data, they are strongly reduced. For the $1s$-state, we find a reduction by about a factor of 1/17. With increasing primary quantum number n this effect is getting less pronounced. E. g., the $4s$-state is reduced only by a factor of about 1/3.

We find that within a given shell (same principal quantum number) the binding energy *increases* with the angular momentum. This quite uncommon behaviour can be demonstrated more clearly for higher shells, which offer a wider range of l-values. Therefore, we display in figure 1 the binding energies of the subshells for $n = 7$ and $n = 8$ for a homogeneously charged sphere in comparison to a point nucleus. While the binding energy increases with increasing angular momentum in case of the extended nucleus, it is the opposite for a point-like nucleus. This leads to an interesting overlap between the energy levels of both shells, e.g. the $8d, 8f$, etc . . . states are more tightly bound than the $7s$ state. The other interesting aspect of the extended nucleus is that within a given shell the difference in energy $E_{n,l} - E_{n,l+1}$ is almost l-independent for the low angular momenta. We find also that $d = E_{n,l} - E_{n+1,l+1}$ does not dependent on n, l quantum numbers. In other words, it behaves like a 3-dimensional harmonic oscillator. We observe also that within a given shell the largest difference between a point-like model and a homogeneous sphere model is seen for the s-states ($l = 0$). That difference decreases with increasing angular momentum. The two models predict the same binding energy for angular momenta equal or larger than $l = 8$. In contrast the difference between the s-states of the two models remains quite large even for relatively large principal quantum numbers (over 20% for $n = 20$). This is because the τ-lepton in a s-state is still spending a sizable fraction of its time inside the nucleus.

We observe a spin-orbit splitting (fine-structure effect) between the $p_{1/2}$ and the $p_{3/2}$ states of the order of 10^{-4} of the binding energy, which is to be compared to a value of about 10^{-1} in case of the point nucleus. This is a further indication that relativistic effects are quite small due to the large τ mass.

In table 2 we compare the binding energies obtained for the homogeneous sphere model using the Dirac equation and the Schrödinger equation [9]. In this table we have set the value of r_0 to 1.1 fm, following Weiss in reference [9] to allow for a better comparison with his non-relativistic data. Everywhere else in this paper we used the value of 1.195788 fm given earlier in this paper. We find an excellent agreement between the non-relativistic

and the relativistic treatments confirming that relativistic effects are quite small and a good treatment of the binding energies of the tauonic atom can be achieved within the framework of the Schrödinger equation. A further extension of the comparison between the relativistic and the non-relativistic wave functions would have been very interesting. Unfortunately, these latter wave functions are presently not available.

Figure 2 shows the variation of K-shell binding energy for electronic, muonic, and tauonic atoms as a function of the atomic number, starting at $Z = 1$ (although we are aware that our model is clearly not realistic for small numbers of Z, since the reduced mass effect has been ignored). The binding energies have been divided by Z and are given in units of the relativistic rest mass mc^2 of the electron, μ, or τ, respectively. As expected, the K-shell binding energy for the electron increases as Z^2 for the low and medium Z atomic numbers and then slightly faster than Z^2 for the high atomic numbers ($Z > 50$). The tauonic curve follows the electronic curve until $Z = 4-5$ above which a much slower dependence than Z^2 is observed. A broad maximum seen around $Z = 20$ translates into a linear dependence while the decrease seen at higher Z values translates into a very slow increase with increasing Z. A consequence of such a weak dependence of the binding energy on the atomic number is that the cross section of bound-free pair production will probably vary less dramatically with the atomic number for the τ than it does for the electron [4,5].

Figure 3 displays the radial components $G(r)$ and $F(r)$ of a τ lepton in the K-shell state for an extended nucleus in comparison to the corresponding wave function in the field of a point charge. We observe that the point nucleus wave function is peaked around 0.15 fm and that its "small" component carries a substantial weight for the density. The corresponding wave function for the extended nucleus shows a very broad distribution with a maximum around 3 fm and the small component carries only a weight of 5.7×10^{-4} to the norm square, which confirms that a treatment within the Schrödinger framework [9] seems to be adequate. About 99% of the density are localized within the equivalence radius of 7.085 fm.

Figure 4 shows $G(r)$ and $F(r)$ of a τ lepton in the $4s_{1/2}$-state, again for an extended nucleus in comparison to a point charge. The slightly reduced influence of the extension of the nucleus as compared to the $1s$-state is reflected in the fact, that the small component of the $4s$-state contributes about 1.28×10^{-3} to the norm square. Here, about 24% of the density are contained within the equivalence radius.

For figure 3 and 4 the Fermi distribution for the nuclear charge has been used. The use of a homogeneously charged sphere results only in very minor changes of the wave functions, which would not be visible in these figures.

It is interesting to note that the finite nuclear size leads to a considerable suppression of the high momentum components contained in the inner-shell wave function. In figure 5 we display the momentum distribution of the $1s$-state, corresponding to a Fermi distribution, a homogeneously charged sphere and a point nucleus. The momentum distribution has been computed by direct numerical Fourier transformation from the coordinate space wave functions [11]. Although we cannot guarantee much accuracy of the momentum space density for $k \geq 1.5$ due to its small value, there is little doubt that the finite nuclear size suppresses the momentum space density by about 8 orders of magnitude or more for $k \geq 1$.

While differences in the wave functions obtained with the Fermi distribution and with the homogeneously charged sphere have not been visible in coordinate space, it is obvious that the suppression of the high momentum components is less pronounced by about 1-2 orders of magnitude in case of the Fermi distribution. Therefore, in the computation of cross sections the more realistic Fermi distribution ought to be employed.

In case of bound-free pair production in relativistic heavy ion collisions with a τ lepton being created in the $1s$-state, the transition amplitudes can be written as an integral over the momentum variable k from $k = E_{1s} + 1 \approx 1.99$ to $k = \infty$ [17]. It is to be expected, that the suppression of the high momentum components we encountered here will be reflected in a corresponding suppression of the transition amplitudes as compared to the transition amplitudes computed with point nucleus wave functions. Bearing in mind that the estimates of cross sections for τ pair production obtained with the point nucleus wave functions are already very small, this additional suppression gives little hope that bound-free τ pair production in relativistic heavy ion collisions will be observable. This leaves us with the pair production in highly energetic photon-ion collisions with the only production mechanism that may be worth further elaboration.

B. Continuum states

In figure 6 we display the radial wave functions for a lead nucleus (Fermi distribution) in comparison with the point nucleus wave function. The energy has been chosen to be $E = -1.04mc^2$ and the angular momentum is zero ($\kappa = -1$). For a continuum state with negative energy, the "large" component $G(r)$ (dotted curve) has a smaller amplitude than the "small" component $F(r)$ (solid curve). Wave functions out of the negative continuum are typically suppressed in the vicinity of the nucleus, which reflects the repulsion of the positive lepton by the nuclear charge. We observe that this suppression is less pronounced for the wave function corresponding to the extended nucleus as compared to the point-like wave function, which is due to the cut-off of the Coulomb singularity. In other words, the extended nucleus acts "less repellent" than the point-like nucleus. In addition, continuum wave functions with higher angular momentum are

even more suppressed around the origin due to the angular momentum term in the radial Dirac equation ("angular momentum barrier"). On the other hand, increasing the kinetic energy of the positive τ counteracts this suppression effect, such that we will observe convergence towards the point-like functions for high kinetic energies of the positive τ, irrespective of the angular momentum.

In spite of this suppression effect, the wave functions out of the negative continuum are reaching their asymptotic behaviour still within the nuclear charge distribution, so that they are quite insensitive to the particular parameter settings of the Fermi-distribution.

Finally, it should be pointed out that - in spite of the minor relevance of relativistic effects for the bound state problem - a fully relativistic treatment of both bound and continuum wave functions is desirable for the computation of cross sections of bound-free transitions, since the use of wave functions which are not exact eigenstates to the same hamiltonian could cause spurious contributions to the computed matrix elements, inducing hardly controllable errors.

ACKNOWLEDGMENTS

We benefited from legacy computer code provided by Prof. Dr. Gerhard Soff. This work was supported by the Director, Office of Energy Research, Office of Basic Energy Sciences, Division of Chemical Sciences, of the U.S. Department of Energy (DOE) under contract No. DE-AC-03-76SF00098.

bound State	a) Fermi distribution	b) homogene sphere	c) point nucleus
$1s_{1/2}$	0.0117865297	0.0117119944	0.198789599
$2s_{1/2}$	0.0087450166	0.0087602565	0.050997786
$2p_{1/2}$	0.0102658819	0.0102191747	0.050997786
$2p_{3/2}$	0.0102641478	0.0102175026	0.045806871
$3s_{1/2}$	0.0062261916	0.0062262795	0.022063559
$3p_{1/2}$	0.0073815096	0.0073765012	0.022063559
$3p_{3/2}$	0.0073801245	0.0073750478	0.020516180
$3d_{3/2}$	0.0087449013	0.0087402579	0.020516180
$3d_{5/2}$	0.0087420161	0.0087375284	0.020094216
$4s_{1/2}$	0.0045430498	0.0045474602	0.012164743
$5s_{1/2}$	0.0034276768	0.0034305167	0.007677200
$6s_{1/2}$	0.0026603798	0.0026619506	0.005277669

TABLE I. Eigenenergies for a τ lepton in an inner shell state of a lead nucleus. The table shows results for 3 different charge distributions, namely a) a 2-parameter Fermi distribution, b) a homogeneously charged sphere and c) a point charge (Sommerfeld's fine structure formula). All energies are given in units of $mc^2 = 1784.2$ MeV.

state	a) Dirac (nlj)	b) Schroedinger (nl)	state	a) Dirac (nlj)	b) Schroedinger (nl)
$1s_{1/2}$	0.012668	0.012684	$6s_{1/2}$	0.002740	0.002830
$2s_{1/2}$	0.009319	0.009431	$6p_{1/2}$	0.003071	0.003170
$2p_{1/2}$	0.010969	0.011037	$6p_{3/2}$	0.003071	
$2p_{3/2}$	0.010967		$6d_{3/2}$	0.003440	0.003548
$3s_{1/2}$	0.006523	0.006662	$6d_{5/2}$	0.003438	
$3p_{1/2}$	0.007771	0.007908	$7p_{1/2}$	0.002411	0.002494
$3p_{3/2}$	0.007769		$7p_{3/2}$	0.002411	
$3d_{3/2}$	0.009290	0.009405	$7d_{3/2}$	0.002662	0.002754
$3d_{5/2}$	0.009287		$7d_{5/2}$	0.002661	
$4s_{1/2}$	0.004721	0.004848	$8d_{3/2}$	0.002119	0.002196
$4p_{1/2}$	0.005484	0.005617	$8d_{5/2}$	0.002119	
$4p_{3/2}$	0.005483		$9d_{3/2}$	0.001726	0.001791
$4d_{3/2}$	0.006399	0.006548	$9d_{5/2}$	0.001726	
$4d_{5/2}$	0.006396				
$5s_{1/2}$	0.003539	0.003646			
$5p_{1/2}$	0.004029	0.004145			
$5p_{3/2}$	0.004028				
$5d_{3/2}$	0.004597	0.004729			
$5d_{5/2}$	0.004596				

TABLE II. Eigenenergies for a τ lepton in an inner shell state of a lead nucleus. The table shows our results for relativistic states with quantum numbers (n,l,j) (a) in comparison to the corresponding non-relativistic data for states with quantum numbers (n,l) (b) given by Weiss. The charge distribution is a homogeneously charged sphere with parameter $r_0 = 1.1fm$. All energies are given in units of $mc^2 = 1784.2$ MeV.

[1] H. Gould: "Atomic Physics Aspects of a Relativistic Heavy Ion Collider", Lawrence Berkeley Laboratory Technical Information, LBL 18593 UC-28, 1984.
[2] C. A. Bertulani and G. Baur, Phys. Rep. **163**, 299 (1988).
[3] M. Fatyga, M. J. Rhoades-Brown, M. J. Tannenbaum, workshop on: "Can RHIC be used to test QED?", April 20-21 1990, BNL 52247 Formal Report.
[4] A. Belkacem, H. Gould, B. Feinberg, R. Bossingham, and W. E. Meyerhof, Phys. Rev. Lett. **71**, 1514 (1993).
[5] A. Belkacem, H. Gould, B. Feinberg, R. Bossingham, and W. E. Meyerhof, Phys. Rev. Lett. **73**, 2432 (1994).
[6] *see, e. g.,* D. C. Ionescu, Phys. Rev. A **49**, 3188 (1994) *and references therein.*
[7] K. Momberger, N. Grün, W. Scheid, U. Becker and G. Soff, J. Phys. B: At. Mol. Phys. **20**, L281 (1987).
[8] J. C. Wells, V. E. Oberacker, A. S. Umar, C. Bottcher, M. R. Strayer, J. S. Wu, G. Plunien, Phys. Rev. A **45**, 6296 (1992).
[9] Morton S. Weiss: "Tau Electron Atoms at RHIC", Lawrence Livermore National Laboratory, Preprint UCRL-93603, 1985.
[10] Y.N. Kim "Mesic Atoms and Nuclear Structure", North-Holland Publishing Company (1971).
[11] H. J. Bär, G. Soff, Physica **128 C**, 225 (1985).
[12] M. E. Rose, "Relativistic Electron Theory" (Wiley, New York, 1961).
[13] S. Cohen, Phys. Rev **118**, 489 (1960).
[14] G. Soff, W. Greiner, W. Betz, B. Müller, Phys. Rev. A **20**, 169, (1979).
[15] G. Mehler, T. de Reus, U. Müller, R. Reinhardt, B. Müller and W. Greiner, Nucl. Inst. and Meth. **A 20**, 559 (1985).
[16] B. Mueller, J. Rafelski and W. Greiner, Nuovo Cimento **A 18**, 551 (1973).
[17] U. Becker, J. Phys. B: At. Mol. Phys. **20**, 6563 (1987).

FIG. 1. Binding energies of tauonic lead in units of mc^2 = 1784.2 MeV for the potential of a homogeneously charged sphere with radius $R_0 = 1.195788fm \times A^{1/3} = 7.085fm$. Displayed are the subshells $n = 7, 8$ with the angular momentum l ranging from 0 to $n-1$. These binding energies are compared to the point nucleus results as given by Sommerfeld's fine structure formula.

FIG. 2. Binding energies for electronic, muonic, and tauonic atoms as a function of the atomic charge number Z in units of the lepton rest mass mc^2 divided by Z. For the muonic and tauonic states, the homogeneous charge distribution has been used with the same parameter settings as in figure 1. The solid curve displays the (Schrödinger-like) Z^2 dependence.

FIG. 3. Radial wave functions $G(r), F(r)$ in tauonic lead for the K-shell state. The solid curves show the radial functions for the extended nucleus, obtained with a Fermi charge distribution with the same parameter settings as in table 1. The dotted curves show the corresponding point nucleus wave function. Natural units have been employed, i.e. length is given in units of $\lambda = 0.1106fm$. The equivalence radius of the charge distribution amounts to $64.06 \times \lambda$.

FIG. 4. Same as figure 3, but for the $4s$-state in tauonic lead.

FIG. 5. Momentum distribution for the $1s$-state in tauonic lead, obtained with a) a Fermi distribution, b) a homogeneously charged sphere, and c) a point nucleus. This demonstrates the suppression of the high momentum components contained in the inner shell state in case of an extended nucleus. Natural units are employed, i.e. momentum is given in units of $\hbar/\lambda$.

FIG. 6. Radial wave functions for tauonic lead (Fermi distribution) in comparison with the point nucleus wave function. The energy is $E = -1.04mc^2$ and the angular momentum is zero ($\kappa = -1$). For a negative energy state, the "large" component $G(r)$ (dotted curve) has a smaller amplitude than the "small" component $F(r)$ (solid curve).

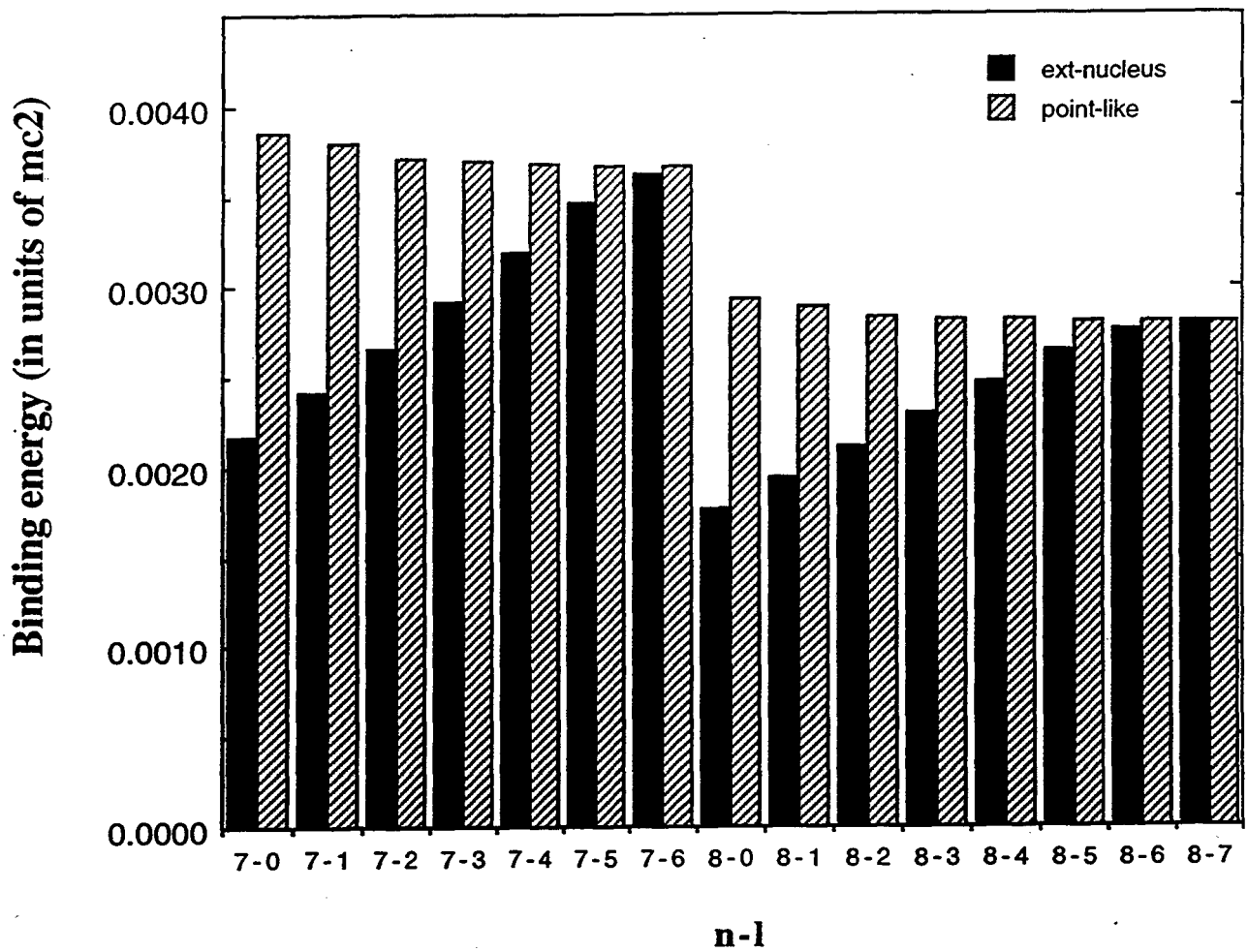
ext-nucleus
point-like
Binding energy (in units of mc2)
0.0040
0.0030
0.0020
0.0010
0.0000
7-0 7-1 7-2 7-3 7-4 7-5 7-6 8-0 8-1 8-2 8-3 8-4 8-5 8-6 8-7
n-l

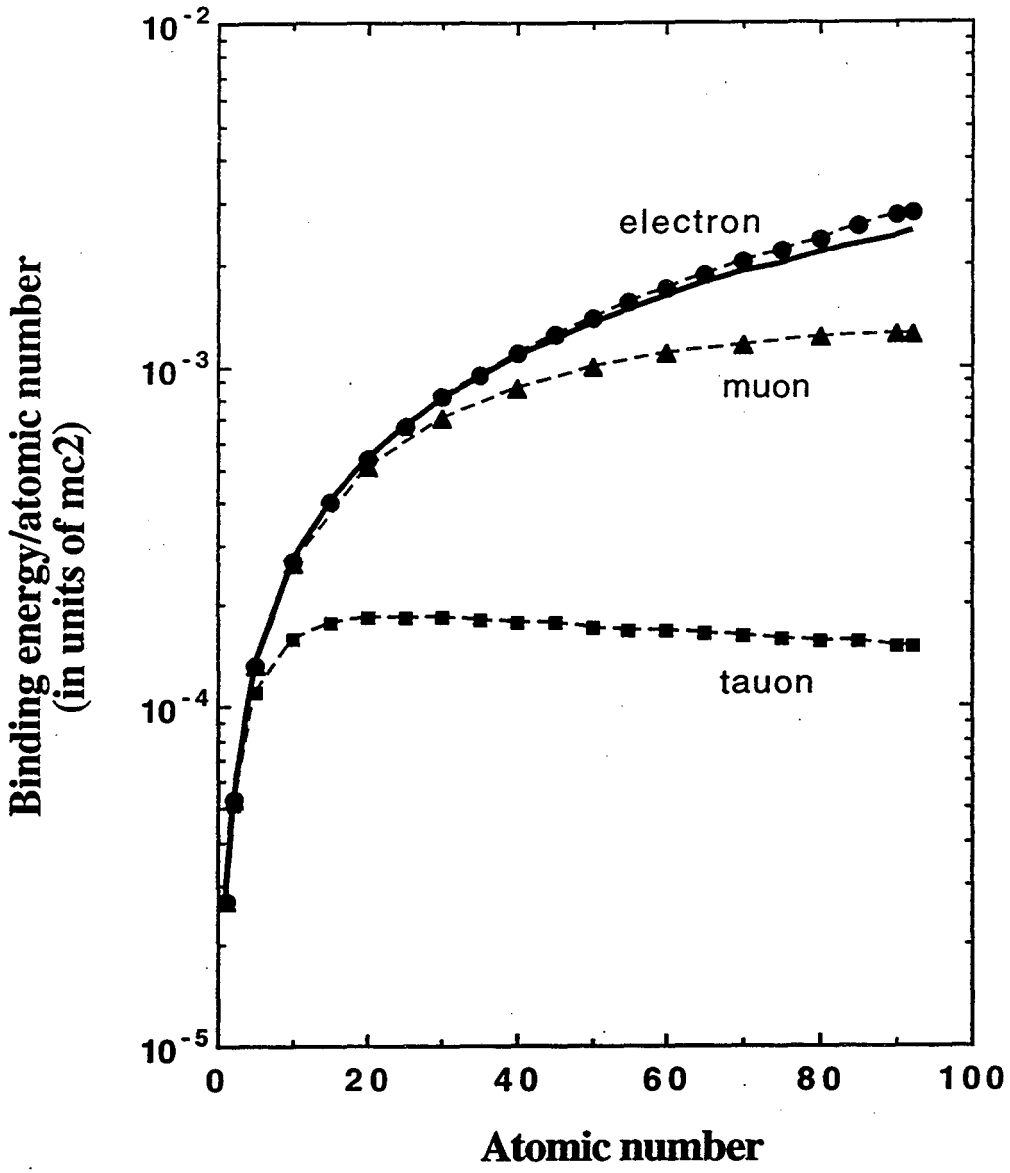
Binding energy/atomic number
(in units of mc2)
10^-2
10^-3
10^-4
10^-5
0
20
40
60
80
100
Atomic number
electron
muon
tauon

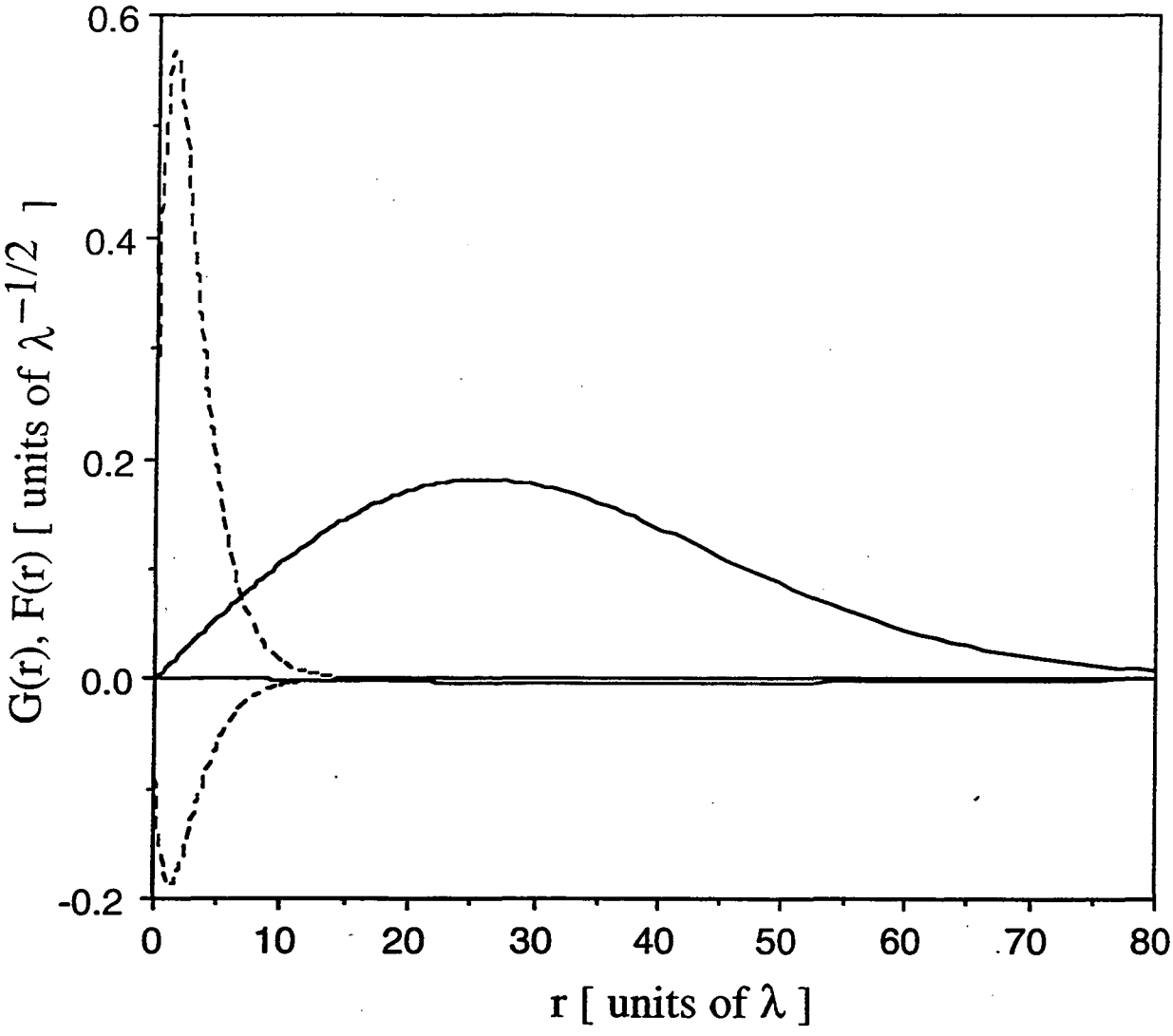
0.6
0.4
0.2
0.0
-0.2
0
10
20
30
40
50
60
70
80
G(r), F(r) [units of λ^−1/2]
r [units of λ]

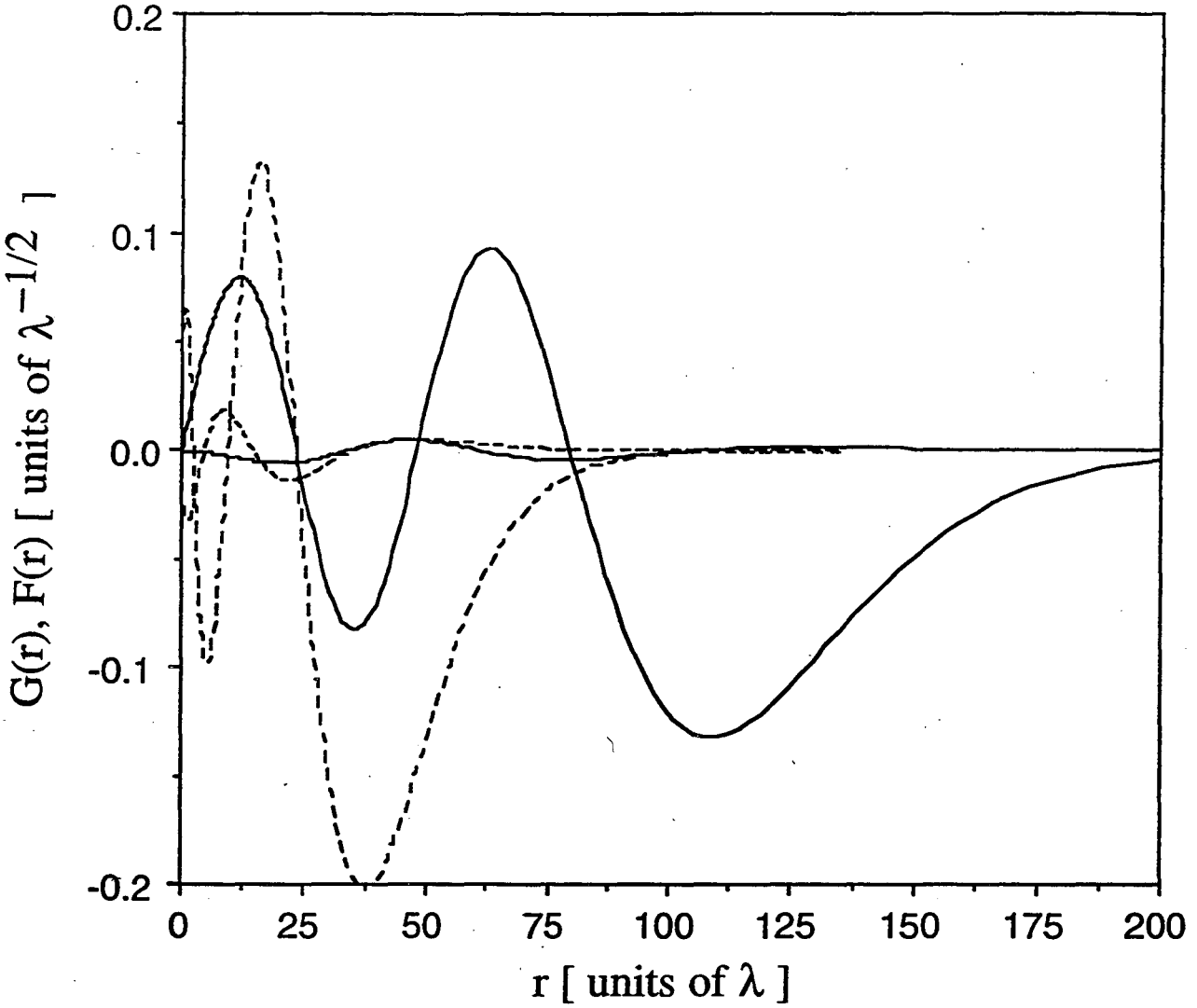
0.2
0.1
0.0
-0.1
-0.2
0
25
50
75
100
125
150
175
200
G(r), F(r) [units of λ−1/2]
r [units of λ]

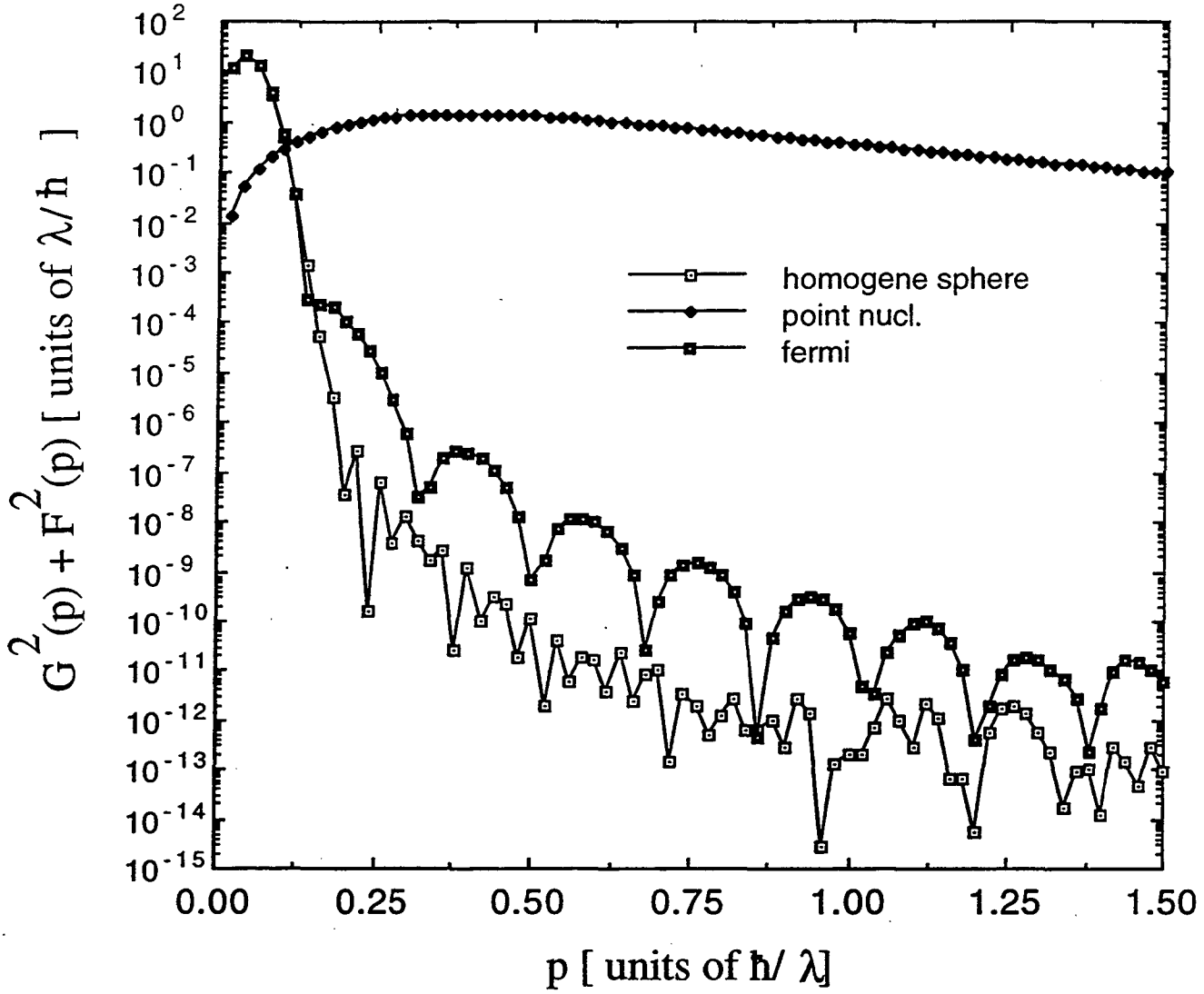
$G^2(p) + F^2(p)$ [units of $\lambda/\hbar$]
10^{2}
10^{1}
10^{0}
10^{-1}
10^{-2}
10^{-3}
10^{-4}
10^{-5}
10^{-6}
10^{-7}
10^{-8}
10^{-9}
10^{-10}
10^{-11}
10^{-12}
10^{-13}
10^{-14}
10^{-15}
0.00
0.25
0.50
0.75
1.00
1.25
1.50
p [units of $\hbar/\lambda$]
homogene sphere
point nucl.
fermi

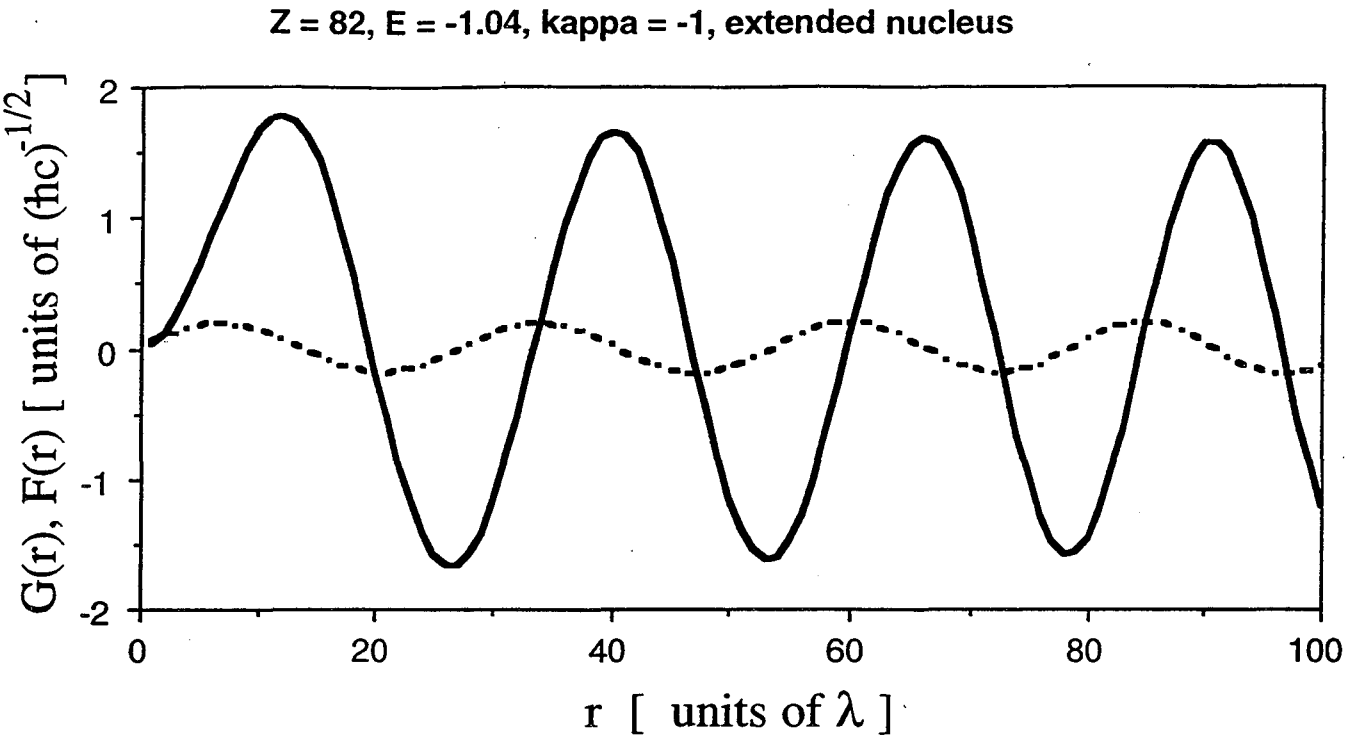
Z = 82, E = -1.04, kappa = -1, extended nucleus
G(r), F(r) [units of (ħc)^-1/2]
2
1
0
-1
-2
0
20
40
60
80
100
r [units of λ]

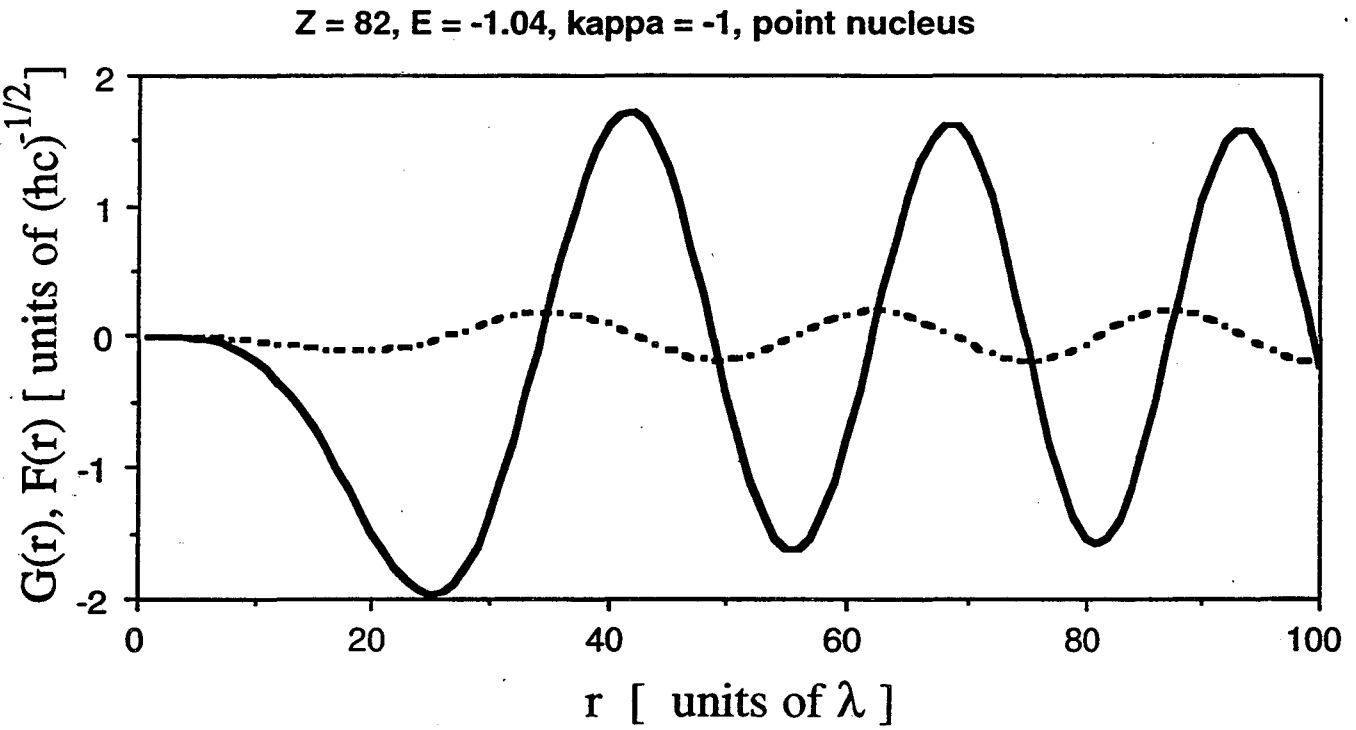
Z = 82, E = -1.04, kappa = -1, point nucleus
G(r), F(r) [units of (ħc)^-1/2]
2
1
0
-1
-2
0
20
40
60
80
100
r [units of λ]

Ernest Orlando Lawrence Berkeley National Laboratory
One Cyclotron Road | Berkeley, California 94720

Prepared for the U.S. Department of Energy under Contract No. DE-AC03-76SF00098